Editors' Suggestion | Featured in Physics

Quantum Flicker Noise in Atomic and Molecular Junctions

Ofir Shein-Lumbroso,[1] Junjie Liu,[2,*] Abhay Shastry,[2,*] Dvira Segal,[2,3,†] and Oren Tal[1,‡]
[1]Department of Chemical and Biological Physics, Weizmann Institute of Science, Rehovot 7610001, Israel
[2]Department of Chemistry and Centre for Quantum Information and Quantum Control, University of Toronto, 80 Saint George Street, Toronto, Ontario M5S 3H6, Canada
[3]Department of Physics, 60 Saint George Street, University of Toronto, Toronto, Ontario M5S 1A7, Canada

(Received 25 July 2021; accepted 2 May 2022; published 9 June 2022)

We report on a quantum form of electronic flicker noise in nanoscale conductors that contains valuable information on quantum transport. This noise is experimentally identified in atomic and molecular junctions and theoretically analyzed by considering quantum interference due to fluctuating scatterers. Using conductance, shot-noise, and flicker-noise measurements, we show that the revealed quantum flicker noise uniquely depends on the distribution of transmission channels, a key characteristic of quantum conductors. This dependence opens the door for the application of flicker noise as a diagnostic probe for fundamental properties of quantum conductors and many-body quantum effects, a role that up to now has been performed by the experimentally less-accessible shot noise.

DOI: 10.1103/PhysRevLett.128.237701

Flicker noise is typically regarded as the most ubiquitous noise in nature (see, e.g., Refs. [1–4]). It is also experimentally accessible and widely studied. However, shot noise is, in fact, the dominant noise used for fundamental characterization of quantum transport and related many-body effects. This is despite the challenges involved in measuring shot noise due to its relative small signal. Specifically, the combination of electronic conductance and shot-noise measurements in quantum coherent conductors has been used extensively to extract information on quantum transport. For example, such measurements play a central role in the analysis of the fractional quantum Hall effect [5,6], Kondo effect [7,8], spin-polarized quantum transport [9–14], electron-phonon interaction [15–18], and in revealing the influence of local atomic structure on the conductance of atomic and molecular junctions [19–24]. Electronic shot noise is a useful source for information, because it depends on the distribution of transmission channels, which determines quantum transport in the framework of Landauer formalism [25]. For $eV \gg k_B T$, the dependence of the power spectral density of shot noise on transmission channels is given by [12,25] $S_{\mathrm{SN}} = 2eIF$, where $F = [\sum_i \tau_i(1-\tau_i)]/\sum_i \tau_i$ is the Fano factor and τ_i is the transmission probability at the Fermi energy of the ith channel (e, electron's charge; V, applied voltage; k_B, Boltzmann's factor; T, temperature; I, current). Considering the distinct dependence of conductance G on transmission channels [25], $G = G_0 \sum_i \tau_i$, where $G_0 = 2e^2/h$ is the conductance quantum (h, Planck's constant), shot noise and conductance can provide information on the distribution of transmission channels in quantum conductors and allow the explorations of many-body interactions in quantum devices.

Electronic flicker noise has been measured in a variety of nanoscale systems (see, e.g., Refs. [26–34]), including atomic and molecular junctions [35–44]. However, the quantum nature of flicker noise as manifested in the relation between this noise and the distribution of transmission channels has not been examined experimentally or theoretically, despite the important role of these channels. Here, we reveal a quantum version of flicker noise with a unique dependence on the channels' transmission probabilities, distinct from the behavior of conductance and shot noise. We use the break junction technique [45] [Fig. 1(a)] to jointly measure conductance, flicker noise, and shot noise in an ensemble of atomic and molecular junctions based on gold (Au) and hydrogen. The relation between the measured flicker noise and transmission channels is analyzed with the aid of a model based on quantum interference in the presence of fluctuating scatterers located near the junction [Fig. 1(a), inset]. Based on the measured flicker noise, shot noise, and conductance, we perform a transmission channel analysis [46], reaching a higher accuracy than when merely using the latter two, as is commonly done. Typically, flicker noise is more experimentally accessible than shot noise. Therefore, the combination of flicker-noise and conductance measurements, or flicker noise, conductance, and shot noise, can promote a more widespread (in the former case) and more accurate (in the latter case) analysis of transmission channels in quantum conductors. Beyond Landauer transport, we anticipate that the revealed nature of flicker noise would provide useful information on Kondo systems, superconducting point contacts, fractional quantum Hall devices, and electron-phonon interaction in atomic-scale junctions.

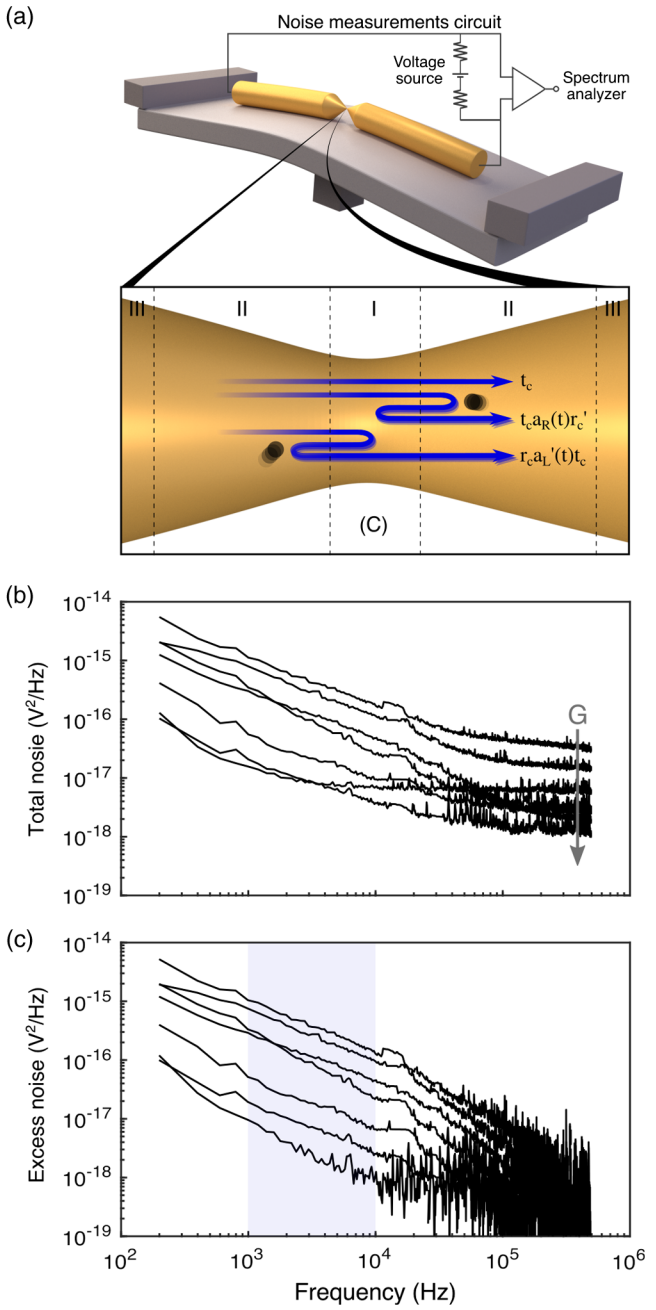

FIG. 1. (a) Illustration of the break-junction setup and measurement circuit. Inset: flicker-noise model. Conducting electrons experience coherent scattering in the atomic-scale junction (I) and by elastic scatterers in (II), resulting in a quantum interference term that contributes to the junction transmission. Fluctuations of the scatterers cross section generate flicker noise with quantum characteristics. (b) Measured total noise vs frequency for seven Au-hydrogen junctions, experiencing 5 mV bias with $0.55 - 7.32G_0$ conductance, top to bottom. (c) Excess noise (practically flicker noise) vs frequency after subtracting thermal and shot noises.

We treat electron transport in an atomic-scale junction at low temperature, using a quantum-coherent wave picture. The junction is separated into three regions [Fig. 1(a), inset]: (I) The central region (C) is of atomic dimensions and supports ballistic transport. (II) To the left and right of region C, we identify the "interface zones," which extend within the coherent mean free path. Scattering processes within these regions are assumed to be elastic and are treated using the coherent scattering approach. Fluctuating defects in the interface zones result in changes to the cross section for electron scattering. These dynamical defects are responsible for the physics of flicker noise in our system. (III) Away from the interface zones, beyond the phase-coherent and elastic mean free path, the rest of the structure is treated as an ideal metal.

Since the dynamics of defects occur on a timescale much longer than that of electron transport through the junction, we derive an expression for flicker noise that depends on the distribution of transmission channels in the framework of Landauer-Büttiker formalism [25]. We follow Ludoph *et al.* [47,48], taking into account the interference of incoming electrons with a wave component that is reflected due to scattering with defects at the interface zones. However, in our model, scatterers have a dynamic scattering cross section. The derived expression

$$S_f(\omega) = S \sum_i \tau_i^2 (1 - \tau_i) \tag{1}$$

provides a quantum version of flicker noise, using $S \equiv 2G_0^2 V^2 \Phi(\omega)$. As seen in Supplemental Material [49], Eq. (1) was obtained after (i) neglecting correlations between different channels and different electrodes and (ii) assuming a power spectrum of reflection amplitudes due to defects in region II, $\Phi(\omega)$, which does not depend on the channel index. Namely, we assume for simplicity that in the multichannel case, electrons in different channels are affected by the same defect configuration. The power spectrum $\Phi(\omega)$ and the transmission probability τ_i are evaluated at the Fermi energy. Equation (1) connects between the measured flicker noise and the microscopic picture of transmission channels, which is the focus of our analysis. Note that this equation can be generalized (Supplemental Material [49]) by allowing the transmission and reflection processes of the central region to be time dependent as well.

Figure 1(b) shows the total noise measured for several Au-hydrogen junctions. The introduction of hydrogen into cold Au atomic-scale junctions (4.2 K) allows us to study flicker noise in a wide conductance range, also below the $\sim 1G_0$ conductance of Au single-atom contacts [47]. To extract the flicker-noise contribution, we subtract unwanted contributions of circuit output voltage noise and amplifier current input noise [56,57]. Furthermore, we correct signal suppression by setup RC filtering (R, resistance; C, capacitance). Finally, we probe the thermal and shot noises at 280–290 kHz, where the flicker noise is negligible, and subtract their contributions from the total measured noise to reveal the flicker-noise component [Fig. 1(c)]. The measured flicker noise depends on the frequency with

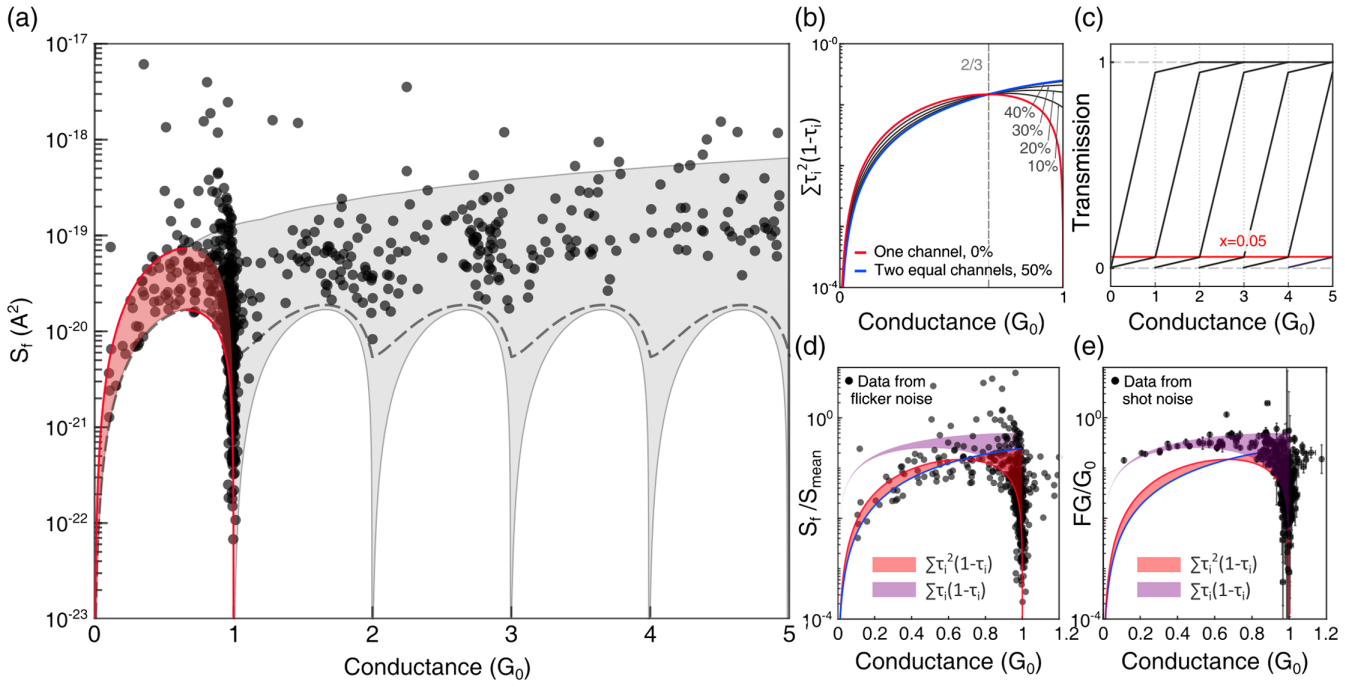

FIG. 2. (a) Flicker noise integrated in $10^3 - 10^4$ Hz vs conductance. Each data point (black) is measured for a different Au-hydrogen junction realization. Note that bare Au forms stable contacts only above $\sim 0.75G_0$ (Supplemental Figs. S4 and S5 [49]). The upper red curve is a fit of $S_f = S_{\max}\tau_1^2(1-\tau_1)$ between 0 and $2/3G_0$, and the lower red curve is a fit to $S_f = S_{\min}\tau_1^2(1-\tau_1)$ between $2/3G_0$ and $1G_0$ (data below 10^{-19} A^2 were considered). The gray area presents the allowed flicker-noise values based on Eq. (1). The lower boundary is relevant for an ideal sequential channel opening, and the dashed black curve provides the lower boundary for the nonideal sequential opening of channels presented in (c). (b) $\sum_i \tau_i^2(1-\tau_i)$ vs conductance for one and two transmission channels. (c) Model for nonideal sequential opening of channels [19]. (d) S_f/S_{mean} vs conductance. Semitransparent red and purple areas are the ensembles of $\sum_i \tau_i^2(1-\tau_i)$ and $\sum_i \tau_i(1-\tau_i)$, respectively, for all possible values of τ_1 and τ_2 for conductance below $1G_0$. (e) Similar to (d), but for FG/G_0. The blue and red curves in (d) and (e) correspond to $\sum_i \tau_i^2(1-\tau_i)$ with two equally opened channels and a single channel, respectively. Data in (a) were converted from V^2 to A^2 by division with the square of the corresponding junction's resistance. Data errors in (a) and (d) are comparable to or smaller than the symbols.

a power that scatters around 1 ($\alpha \cong 1$, using Hooge's expression [58] $S_f \sim 1/f^\alpha$) and shows a typical quadratic dependence on voltage in the examined mV range. Finally, we integrate over the noise in the range of $10^3 - 10^4$ Hz, shaded in Fig. 1(c) (Supplemental Material [49]).

The integrated noise S_f for 623 junctions with different conductance values is presented in Fig. 2(a). In what follows, we analyze these data in view of Eq. (1). As a first step, we focus on the S prefactor. $\Phi(\omega)$ may vary between junctions, since it is sensitive to the details of the fluctuating scatterers that can be different for different junctions. As a result, S has a range that can be characterized by $S_{\min}$ and $S_{\max}$. These coefficients are setup specific. For example, in cleaner materials with fewer defects, their values would be smaller. To find $S_{\min}$ and $S_{\max}$, we focus on noise data between 0.1 and $1G_0$, for which former shot-noise measurements on Au-hydrogen junctions [57] revealed conductance dominated by a single transmission channel, while a minor contribution from a second channel (or more in rare cases) was found when the conductance approached $1G_0$, probably due to direct Au-Au tunneling.

Figure 2(b) illustrates that below $2/3G_0$, the expression $\sum_i \tau_i^2(1-\tau_i)$ is maximal if a single channel contributes (red curve). In contrast, between $2/3$ and $1G_0$, a single channel leads to minimal flicker noise (red curve), compared to multichannel junctions. Consequentially, we can fit the lowest data points between $2/3$ and $1G_0$ in Fig. 2(a) to $S\tau^2(1-\tau)$, with $\tau = G/G_0$, and extract $S_{\min}$. We repeat the fitting for the highest data points below $2/3G_0$ to obtain $S_{\max}$ (red curves). The semitransparent red region in Fig. 2(a) describes the expected flicker noise for a single transmission channel with S between $S_{\max}$ and $S_{\min}$ due to variations in the scatterers' distribution for different junctions. The data spread above the semitransparent red region increases as the conductance approaches $1G_0$. This trend is ascribed to the contribution of more than a single transmission channel (Supplemental Fig. S6 [49]). The gray region in Fig. 2(a) was generated by allowing different transmission partitions and using $S_{\min}$ and $S_{\max}$. It describes the area where we expect to find flicker-noise data. The upper limit of flicker noise according to Eq. (1) is depicted by the upper boundary of the gray area. Along this curve, which is approximately proportional to $G/4$, the

conductance is made of equal transmission probabilities. Namely, for N channels, $\tau_1 = \tau_2 = \cdots = \tau_N = G/(NG_0)$ (Supplemental Material [49]).

The appearance of some data points above this curve (e.g., 7% of the points between 0.9 and $1.0G_0$) can indicate additional noise contributions that are not described by Eq. (1), such as conductance fluctuations due to junction instability. The bottom boundary of the gray region presents the lower limit of flicker noise based on Eq. (1) for the case of sequential opening of channels, as expected for an ideal quantum point contact [59]. Specifically, it is given by one channel up to $1G_0$ with $\tau_1 = G/G_0$. For higher conductance, a second channel is opened while the first channel remains fully open with $\tau_1 = 1$ and $\tau_2 = G/G_0 - 1$ up to $2G_0$, etc. However, for Au atomic contacts (with or without hydrogen), the opening of channels when the conductance increases is not fully sequential. Namely, before a given channel is fully open ($\tau_i = 1$), another channel or more are already partially opened (e.g., $0 < \tau_{i+1} < 1$) [19,46,60]. Considering the channel evolution in Fig. 2(c) (suggested in Ref. [19]), Eq. (1) yields a lower limit for flicker noise seen as a dashed black curve in Fig. 2(a). This curve describes better the minimal values of the measured flicker noise. In reality, the number of partially open channels slightly increases as the conductance increases [46,60,61]. Consequentially, the lower boundary for the measured flicker noise should slightly increase at higher conductance and deviate from the dashed curve, as indeed seen in Fig. 2(a) above $\sim 3G_0$.

By combining measurements of flicker noise and shot noise on the same junctions, we check if the two types of probed noise indeed reveal distinctive dependence on the channel distribution, as expected by the theoretical treatment. This dependence can be expressed as $S_f/S = \sum_i \tau_i^2(1-\tau_i)$ for flicker noise and $FG/G_0 = \sum_i \tau_i(1-\tau_i)$ for shot noise. Figures 2(d) and 2(e) present the measured S_f/S and FG/G_0 (black dots). For the prefactor S, we use $S_{\mathrm{mean}} = (S_{\mathrm{min}} + S_{\mathrm{max}})/2)$. On top of these normalized experimental data, we present the calculated $\sum_i \tau_i^2(1-\tau_i)$ in red and $\sum_i \tau_i(1-\tau_i)$ in purple, assuming up to two channels with all possible combinations of τ_1 and τ_2 that satisfy $G = G_0(\tau_1 + \tau_2)$. As can be seen, the center of the measured S_f/S is well described by $\sum_i \tau_i^2(1-\tau_i)$, as expected when using S_{mean}, and the measured FG/G_0 is captured by $\sum_i \tau_i(1-\tau_i)$. This analysis verifies that the probed flicker noise and shot noise are two independent functions of the channel's transmission probabilities.

The distinct dependence of conductance and shot noise on transmission channels has been employed for channel analysis [9–24]. However, using two independent equations (for conductance and shot noise) discloses analytically only up to two transmission probabilities. This limitation is partially lifted by adopting numerical approaches that provide information on the transmission probabilities of more than two channels, with the cost of reduced accuracy [46]. Thanks to the flicker-noise dependence on the channel distribution, we can now utilize flicker noise for channel analysis. Figure 3(a) presents the Fano factor extracted from shot-noise measurements of Au-hydrogen junctions as a function of conductance, where each data point was measured on a different junction. To examine the use of flicker noise in numerical channel analysis, which is usually based merely on conductance and shot noise, we focus in Fig. 3(a) on two data points labeled as I and II. Figure 3(b) presents the transmission probabilities of the four most dominant channels. The blue distributions indicate the possible range of transmission probabilities τ_i, based on shot-noise and conductance analysis (relevant values are given in Table I). For example,

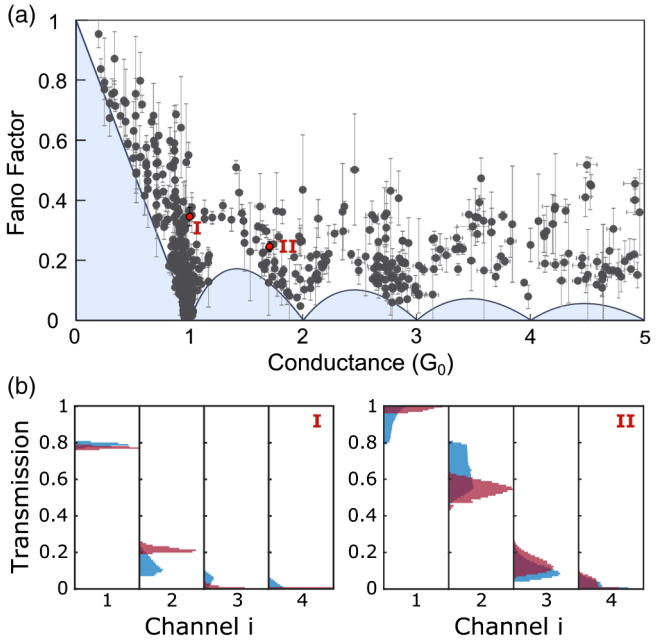

FIG. 3. (a) Fano factor vs conductance for 860 Au-hydrogen junctions. (b) Two examples I and II, for numerical channel analysis based on conductance and shot noise (blue) and conductance, shot noise, and flicker noise (red) for the most dominant four transmission channels. The Fano factor vs conductance data are marked as I and II in (a). The distributions' width provides the range of possible transmission for each channel, and the amplitude indicates the relative probability of the transmission values. Table I presents relevant parameters for the two examples, where $S_f(\mathrm{I}) = 8.52 \times 10^{-20}$ A^2 and $S_f(\mathrm{II}) = 2.13 \times 10^{-20}$ A^2. Using $S_{\mathrm{max}} = 5.01 \times 10^{-19}$ A^2 and $S_{\mathrm{min}} = 1.12 \times 10^{-19}$ A^2, we reach the range of S_f/S in Table I.

TABLE I. Parameters for channel analysis.

	I	II
$G/G_0 = \sum \tau_i$	1.00 ± 0.01	$1.71 + 0.01$
$F = \sum \tau_i(1-\tau_i)/\sum \tau_i$	0.35 ± 0.03	0.24 ± 0.02
$S_f/S = \sum \tau_i^2(1-\tau_i)$	0.17-0.76	0.04-0.19

the second channel of junction I has a transmission probability between $0.06 \leq \tau_2 \leq 0.26$, where the uncertainty comes from the application of two equations to obtain information on four transmission probabilities [46]. The red distributions are calculated based on flicker-noise, shot-noise, and conductance data (Table I). Proceeding with our example, this analysis yields a transmission probability for the second channel of junction I in the range of $0.19 \leq \tau_2 \leq 0.26$, namely, with a reduced uncertainty. Similarly, the analysis of other transmission channels in Fig. 3(b) shows that considering flicker-noise data on top of conductance and shot-noise data leads to improved accuracy (generally, the accuracy can be better or equal).

Shot-noise measurements are typically demanding due to relatively low signals. In contrast, flicker-noise measurements offer a more experimentally accessible approach for channel analysis. Furthermore, flicker noise is often collected as a side effect of shot-noise measurements. In these cases, it can serve fruitfully, with shot noise, for a more accurate channel analysis without setup adjustments. To probe the span of flicker noise for different junction geometries and distributions of fluctuating scatterers, we deliberately crashed the electrodes against each other between junction realizations. A moderate or no crash can minimize S variations by preserving the characteristics of fluctuating scatterers near the junction, thus achieving a more accurate analysis in break-junction experiments. Note that ensemble-averaged conductance fluctuations measured for thousands of junctions have shown a similar *collective* dependence on channels as found here for flicker noise due to a similar origin [47,48]. However, while this approach probes ensemble-averaged properties, it cannot be utilized for channel analysis in individual quantum conductors, in contrast to conductance, shot-noise, and flicker-noise measurements.

The quantum version of flicker noise [Eq. (1)] is generally valid for any phase-coherent quantum electronic conductor when dynamical scatterers are active. At the tunneling limit for a single channel, flicker noise can be used to extract the charge of quasiparticles, thus providing an independent probe that complements shot-noise analysis of quasiparticles and electron-electron interactions. Beyond charge transport analysis, flicker noise can now be used to analyze spin transport by determining the conductance spin polarization [9–14]. Finally, electron-phonon interactions are extensively studied in atomic and molecular junctions [62–81]. Considering Eq. (1), for a transmission probability smaller (larger) than $2/3$, flicker noise should increase (decrease) when a phonon mode is activated (Supplemental Material [49]). This response can provide an analysis tool for the study of electron-phonon interactions in atomic-scale conductors.

D. S. acknowledges the Natural Sciences and Engineering Research Council of Canada (NSERC) discovery grant and the Canada Research Chair Program. O. T. appreciates the support of the Harold Perlman family, and acknowledges funding by research grants from Dana and Yossie Hollander, and the European Research Council (Grant No. 864008).

*These authors contributed equally to this work.
†dvira.segal@utoronto.ca
‡oren.tal@weizmann.ac.il

[1] P. Dutta and P. M. Horn, Rev. Mod. Phys. **53**, 497 (1981).
[2] P. Bak, C. Tang, and K. Wiesenfeld, Phys. Rev. Lett. **59**, 381 (1987).
[3] D. L. Gilden, T. Thornton, and M. W. Mallon, Science **267**, 1837 (1995).
[4] W. Li and D. Holste, Phys. Rev. E **71**, 041910 (2005).
[5] L. Saminadayar, D. C. Glattli, Y. Jin, and B. Etienne, Phys. Rev. Lett. **79**, 2526 (1997).
[6] R. de Picciotto, M. Reznikov, M. Heiblum, V. Umansky, G. Bunin, and D. Mahalu, Nature (London) **389**, 162 (1997).
[7] O. Zarchin, M. Zaffalon, M. Heiblum, D. Mahalu, and V. Umansky, Phys. Rev. B **77**, 241303(R) (2008).
[8] T. Delattre *et al.*, Nat. Phys. **5**, 208 (2009).
[9] P. Roche, J. Ségala, D. C. Glattli, J. T. Nicholls, M. Pepper, A. C. Graham, K. J. Thomas, M. Y. Simmons, and D. A. Ritchie, Phys. Rev. Lett. **93**, 116602 (2004).
[10] L. DiCarlo, Y. Zhang, D. T. McClure, D. J. Reilly, C. M. Marcus, L. N. Pfeiffer, and K. W. West, Phys. Rev. Lett. **97**, 036810 (2006).
[11] M. Kumar, O. Tal, R. H. M. Smit, A. Smogunov, E. Tosatti, and J. M. van Ruitenbeek, Phys. Rev. B **88**, 245431 (2013).
[12] A. Burtzlaff, A. Weismann, M. Brandbyge, and R. Berndt, Phys. Rev. Lett. **114**, 016602 (2015).
[13] R. Vardimon, M. Klionsky, and O. Tal, Nano Lett. **15**, 3894 (2015).
[14] A. N. Pal, D. Li, S. Sarkar, S. Chakrabarti, A. Vilan, L. Kronik, A. Smogunov, and O. Tal, Nat. Commun. **10**, 5565 (2019).
[15] O. Tal, M. Krieger, B. Leerink, and J. M. van Ruitenbeek, Phys. Rev. Lett. **100**, 196804 (2008).
[16] M. Kumar, R. Avriller, A. L. Yeyati, and J. M. van Ruitenbeek, Phys. Rev. Lett. **108**, 146602 (2012).
[17] R. Ben-Zvi, R. Vardimon, T. Yelin, and O. Tal, ACS Nano **7**, 11147 (2013).
[18] S. G. Bahoosh, M. A. Karimi, W. Belzig, E. Scheer, and F. Pauly, arXiv:1912.13496.
[19] H. E. van den Brom and J. M. van Ruitenbeek, Phys. Rev. Lett. **82**, 1526 (1999).
[20] D. Djukic and J. M. van Ruitenbeek, Nano Lett. **6**, 789 (2006).
[21] M. Kiguchi, O. Tal, S. Wohlthat, F. Pauly, M. Krieger, D. Djukic, J. C. Cuevas, and J. M. van Ruitenbeek, Phys. Rev. Lett. **101**, 046801 (2008).
[22] P. J. Wheeler, J. N. Russom, K. Evans, N. S. King, and D. Natelson, Nano Lett. **10**, 1287 (2010).
[23] R. Vardimon, T. Yelin, M. Klionsky, S. Sarkar, A. Biller, L. Kronik, and O. Tal, Nano Lett. **14**, 2988 (2014).
[24] M. A. Karimi, S. G. Bahoosh, M. Herz, R. Hayakawa, F. Pauly, and E. Scheer, Nano Lett. **16**, 1803 (2016).

[25] Y. M. Blanter and M. Büttiker, Phys. Rep. **336**, 1 (2000).
[26] C. Dekker, A. J. Scholten, F. Liefrink, R. Eppenga, H. van Houten, and C. T. Foxon, Phys. Rev. Lett. **66**, 2148 (1991).
[27] J. P. Hessling and Y. M. Galperin, Phys. Rev. B **52**, 5082 (1995).
[28] P. G. Collins, M. S. Fuhrer, and A. Zettl, Appl. Phys. Lett. **76**, 894 (2000).
[29] Y. M. Lin, J. Appenzeller, J. Knoch, Z. Chen, and P. Avouris, Nano Lett. **6**, 930 (2006).
[30] Y. M. Lin and P. Avouris, Nano Lett. **8**, 2119 (2008).
[31] Z. Cheng, Q. Li, Z. Li, Q. Zhou, and Y. Fang, Nano Lett. **10**, 1864 (2010).
[32] W. Yi, S. E. Savel'Ev, G. Medeiros-Ribeiro, F. Miao, M. X. Zhang, J. J. Yang, A. M. Bratkovsky, and R. S. Williams, Nat. Commun. **7**, 11142 (2016).
[33] P. Puczkarski, Q. Wu, H. Sadeghi, S. Hou, A. Karimi, Y. Sheng, J. H. Warner, C. J. Lambert, G. A. D. Briggs, and J. A. Mol, ACS Nano **12**, 9451 (2018).
[34] B. Sánta, Z. Balogh, A. Gubicza, L. Pósa, D. Krisztián, G. Mihály, M. Csontos, and A. Halbritter, Nanoscale **11**, 4719 (2019).
[35] Z. M. Wu, S. M. Wu, S. Oberholzer, M. Steinacher, M. Calame, and C. Schonenberger, Phys. Rev. B **78**, 235421 (2008).
[36] Y. Kim, H. Song, D. Kim, T. Lee, and H. Jeong, ACS Nano **4**, 4426 (2010).
[37] R. Chen, P. J. Wheeler, and D. Natelson, Phys. Rev. B **85**, 235455 (2012).
[38] V. A. Sydoruk, D. Xiang, S. A. Vitusevich, M. V. Petrychuk, A. Vladyka, Y. Zhang, A. Offenhäusser, V. A. Kochelap, A. E. Belyaev, and D. Mayer, J. Appl. Phys. **112**, 014908 (2012).
[39] T. W. Hwang, S. P. Branagan, and P. W. Bohn, J. Am. Chem. Soc. **135**, 4522 (2013).
[40] O. Adak, E. Rosenthal, J. Meisner, E. F. Andrade, A. N. Pasupathy, C. Nuckolls, M. S. Hybertsen, and L. Venkataraman, Nano Lett. **15**, 4143 (2015).
[41] A. Magyarkuti, O. Adak, A. Halbritter, and L. Venkataraman, Nanoscale **10**, 3362 (2018).
[42] D. Cho, S. Shekhar, H. Lee, and S. Hong, Nano Lett. **18**, 1001 (2018).
[43] M. H. Garner, H. Li, Y. Chen, T. A. Su, Z Shangguan, D. W. Paley, T. Liu, F. Ng, H. Li, S. Xiao, and C. Nuckolls, Nature (London) **558**, 415 (2018).
[44] S. Yuan, T. Gao, W. Cao, Z. Pan, J. Liu, J. Shi, and W. Hong, Small Methods **5**, 2001064 (2021).
[45] C. J. Muller, J. M. van Ruitenbeek, and L. J. de Jongh, Phys. Rev. Lett. **69**, 140 (1992).
[46] R. Vardimon, M. Klionsky, and O. Tal, Phys. Rev. B **88**, 161404(R) (2013).
[47] B. Ludoph, M. H. Devoret, D. Esteve, C. Urbina, and J. M. van Ruitenbeek, Phys. Rev. Lett. **82**, 1530 (1999).
[48] B. Ludoph and J. M. van Ruitenbeek, Phys. Rev. B **61**, 2273 (2000).
[49] See Supplemental Material at http://link.aps.org/supplemental/10.1103/PhysRevLett.128.237701 for additional details on the experimental procedure, supplementary experimental data, a derivation of the expression for flicker noise in atomic-scale junctions (part II on theoretical derivations), and supplementary theoretical information. Supplemental Material includes Refs. [50–55], not mentioned in the Letter.
[50] I. Eliazar and J. Klafter, Proc. Natl. Acad. Sci. U.S.A. **106**, 12251 (2009).
[51] M. Niemann, H. Kantz, and E. Barkai, Phys. Rev. Lett. **110**, 140603 (2013).
[52] G. Margolin and E. Barkai, J. Stat. Phys. **122**, 137 (2006).
[53] Sh. Kogan, *Electronic Noise and Fluctuations in Solids* (Cambridge University Press, Cambridge, England, 1996).
[54] A. A. Balandin, Nat. Nanotechnol. **8**, 549 (2013).
[55] S. Engelberg, *A Mathematical Introduction to Control Theory* (Imperial College Press, London, 2005).
[56] A. Kumar, L. Saminadayar, D. C. Glattli, Y. Jin, and B. Etienne, Phys. Rev. Lett. **76**, 2778 (1996).
[57] O. Shein-Lumbroso, L. Simine, A. Nitzan, D. Segal, and O. Tal, Nature (London) **562**, 240 (2018).
[58] M. B. Weissman, Rev. Mod. Phys. **60**, 537 (1988).
[59] B. J. van Wees, H. van Houten, C. W. J. Beenakker, J. G. Williamson, L. P. Kouwenhoven, D. van der Marel, and C. T. Foxon, Phys. Rev. Lett. **60**, 848 (1988).
[60] J. Burki and C. A. Stafford, Phys. Rev. Lett. **83**, 3342 (1999).
[61] M. Dreher, F. Pauly, J. Heurich, J. C. Cuevas, E. Scheer, and P. Nielaba, Phys. Rev. B **72**, 075435 (2005); F. Pauly, J. K. Viljas, M. Bürkle, M. Dreher, P. Nielaba, and J. C. Cuevas, Phys. Rev. B **84**, 195420 (2011).
[62] B. C. Stipe, M. A. Rezaei, and W. Ho, Science **280**, 1732 (1998).
[63] H. Park, J. Park, A. K. L. Lim, E. H. Anderson, A. P. Alivisatos, and P. L. McEuen, Nature (London) **407**, 57 (2000).
[64] N. Agraït, C. Untiedt, G. Rubio-Bollinger, and S. Vieira, Phys. Rev. Lett. **88**, 216803 (2002).
[65] R. H. M. Smit, Y. Noat, C. Untiedt, N. D. Lang, M. C. van Hemert, and J. M. van Ruitenbeek, Nature (London) **419**, 906 (2002).
[66] M. Galperin, M. A. Ratner, and A. Nitzan, J. Chem. Phys. **121**, 11965 (2004).
[67] M. Paulsson, T. Frederiksen, and M. Brandbyge, Phys. Rev. B **72**, 201101(R) (2005).
[68] J. K. Viljas, J. C. Cuevas, F. Pauly, and M. Häfner, Phys. Rev. B **72**, 245415 (2005).
[69] L. de la Vega, A. Martín-Rodero, N. Agraït, and A. Levy Yeyati, Phys. Rev. B **73**, 075428 (2006).
[70] M. Galperin, A. Nitzan, and M. A. Ratner, Phys. Rev. B **74**, 075326 (2006).
[71] T. Frederiksen, N. Lorente, M. Paulsson, and M. Brandbyge, Phys. Rev. B **75**, 235441 (2007).
[72] M. Paulsson, T. Frederiksen, H. Ueba, N. Lorente, and M. Brandbyge, Phys. Rev. Lett. **100**, 226604 (2008).
[73] R. Egger and A. O. Gogolin, Phys. Rev. B **77**, 113405 (2008).
[74] S. Monturet and N. Lorente, Phys. Rev. B **78**, 035445 (2008).
[75] O. Entin-Wohlman, Y. Imry, and A. Aharony, Phys. Rev. B **80**, 035417 (2009).
[76] T. L. Schmidt and A. Komnik, Phys. Rev. B **80**, 041307(R) (2009).
[77] R. Avriller and A. Levy Yeyati, Phys. Rev. B **80**, 041309(R) (2009).

[78] F. Haupt, T. Novotný, and W. Belzig, Phys. Rev. Lett. **103**, 136601 (2009).
[79] F. Haupt, T. Novotný, and W. Belzig, Phys. Rev. B **82**, 165441 (2010).
[80] R. Avriller and T. Frederiksen, Phys. Rev. B **86**, 155411 (2012).
[81] B. Dong, G. H. Ding, and X. L. Lei, Phys. Rev. B **88**, 075414 (2013).